PROCEEDINGS OF SCIENCE

Design considerations for the Micro Vertex Detector of the Compressed Baryonic Matter experiment

M. Deveaux*
Goethe University Frankfurt
E-mail: deveaux@physik.uni-frankfurt.de

S. Amar-Youcef

IPHC Strasbourg, GSI Darmstadt, Goethe University Frankfurt

C. Dritsa

IPHC Strasbourg, GSI Darmstadt, Goethe University Frankfurt

I. Fröhlich

Goethe University Frankfurt

C. Müntz

Goethe University Frankfurt

S. Seddiki

IPHC Strasbourg, Goethe University Frankfurt

J. Stroth

Goethe University Frankfurt

T. Tischler

Goethe University Frankfurt

C. Trageser

Goethe University Frankfurt

The CBM experiment will investigate heavy-ion collisions at beam energies from 8 to 45 AGeV at the future accelerator facility FAIR. The goal of the experiment is to study the QCD phase diagram in the region of moderate temperatures and highest net-baryon densities in search of the first-order phase transition from confined to deconfined matter at the QCD critical point. To do so, CBM aims to measure rare hadronic, leptonic and photonic probes among them open charm. In order to reject the rich background generated by the heavy ion collisions, a micro vertex detector (MVD) providing an unprecedented combination of high rate capability and radiation hardness, very light material budget and excellent granularity is required. In this work, we will present and discuss the concept of this detector.

17th International Workshop on Vertex detectors
July 28 - 1 August 2008
Uto Island, Sweden

PoS(VERTEX 2008)028

1. Introduction

1.1 CBM, a FAIR experiment

The FAIR facility at GSI [1] will offer unique possibilities for the investigation of the QCD phase diagram in the regime of large net-baryon densities, besides serving a variety of other fields of physics with i) anti-proton beams for hadron physics, ii)radioactive beams for nuclear structure physics, and iii) highly pulsed ion beams for plasma physics. For the nuclear collision program, a synchrotron with 300 Tm bending power (SIS-300) will deliver fully stripped heavy ion beams up to uranium with intensities of up to $2 \cdot 10^9$ per second at beam energies from 8 to 35 AGeV. Lighter ions (Z/A = 0.5) can be accelerated up to 45 AGeV, while proton beams will be available up to 90 GeV. The unprecedented beam intensities will allow studying extremely rare probes with high precision but also constitute a high challenge for detectors and electronics. The CBM (Compressed Baryonic Matter) experiment [2] will be a next-generation fixed target detector to be operated at the FAIR heavy-ion synchrotron SIS-300. It is designed to measure hadronic, leptonic and photonic probes in a large acceptance and at the extreme interaction rates offered by the accelerator. CBM aims at a systematic investigation of A+A, p+A and p+p collisions, in terms of collision energy ($\sqrt{S_{NN}} = 4.5 - 9.3$ GeV for heavy nuclei) and system size, with high precision and statistics. In contrast to the low-energy programs at the RHIC and the SPS, which due to low collision rates will focus on bulk particle production, CBM will put special emphasis on the measurement of extremely rare probes which have not been accessible by previous heavy-ion experiments at the AGS and the SPS.

The observables to be covered by CBM include multiplicities, phase space distributions and the flow of strange, multi-strange (K, ϕ,Λ, Ξ, Ω) and charmed hadrons (D, D_S,Λ_C). Short lived vector mesons and charmonium states will be investigated via their di-leptonic decay. The measurements on charmonium states together with open charm measurements will allow a comprehensive study of charm production near the production threshold. Signatures of the critical point will be looked for in event-by-event fluctuations of the quantities like particle yield ratios, charged multiplicity or average p_t.

The envisaged measurements of rare probes calls for an unique instrument providing simultaneously an outstanding rate capability and precision. Combining both is the central design challenge of the CBM experiment. Our global design concept is discussed in [3]. This work will concentrate on the measurement of open charm particles and on the Micro Vertex Detector of CBM. To do so, in section 1.2, we will introduce the global geometry of the the MVD of CBM. Hereafter, in section 2, we will first discuss in detail the requirements on the detector system. In section 3, we will motivate our technology choices and discuss the constraints arising from the features and limits of our guide line technology, which are CMOS Monolithic Active Pixel Sensors. Knowing those constraints, we will introduce the design of our detector ladders and estimate its material budget (section 4). Finally, in section 5, we will propose a running scenario and show some preliminary simulation results of the physics performances of CBM in the field of open charm reconstruction.

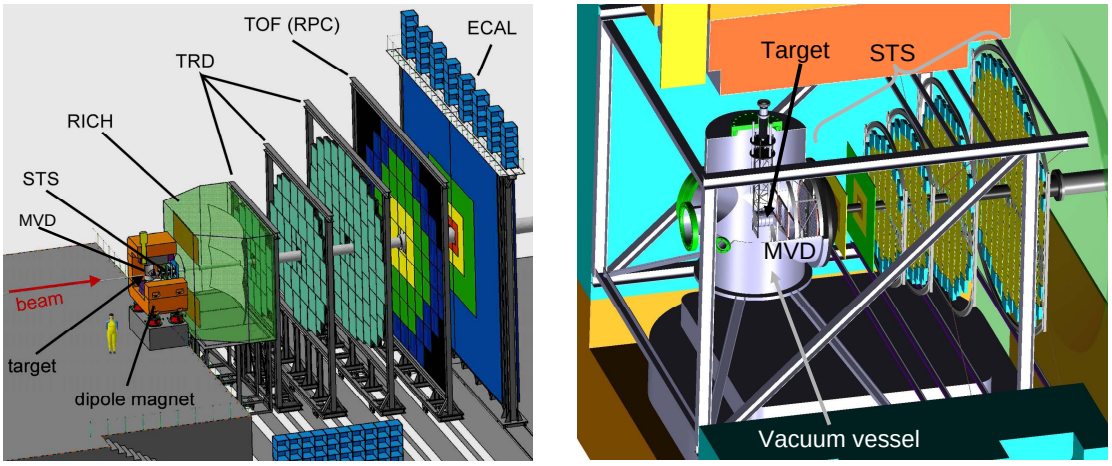

Figure 1: *Artistic view of the global layout of CBM (left) and a zoom into the MVD and STS (right).*

1.2 The CBM Micro Vertex Detector (MVD)

The CBM experiment is currently planned with two configurations among which one is optimized for di-electron spectroscopy and one for di-muon spectroscopy. Open charm measurements will presumably rely on the CBM di-electron setup shown in Figure 1 (left). This setup is formed by a Micro Vertex Detector (MVD) and a Silicon Tracking System (STS), which operate in a 1 Tm magnetic field. Electron identification is provided by a RICH at lower particle energies and by a set of Transitions Radiation Detectors (TDR) at higher energies. A Time-Of-Flight (TOF) system aims for the identification of hadrons with low and medium energies. The setup is completed by an electro magnetic calorimeter, which allows the measurement of direct photons and by a forward hadronic calorimeter (not shown), which measures the energy of spectators of the nuclear collision.

Figure 1 (right) shows a zoom into the region of MVD and STS. Both systems are formed by planar detectors. The outer acceptance angle of both detector system (and all CBM) is given with $\vartheta = 25^\circ$ with respect to the beam axis. An inner opening of the detector stations, which is to allow for a passage of the beam pipe, limits the inner acceptance of the experiment to $\vartheta = 2.5^\circ$. The MVD will operate in the moderate vacuum of the beam pipe which might be separated from the vacuum of the SIS300 synchrotron by differential pumping or a thin foil located afar from the experiment in the beam pipe. The aim of this concept is to avoid unwanted multiple scattering of the particle tracks in a vacuum window located between the target and the MVD. In our concept, this vacuum window will be located between the MVD and the STS. The latter operates in the cooled atmosphere required for avoiding unwanted radiation damage effects like intense leakage currents or reverse annealing in the silicon strips.

The details of both, the MVD and the STS, are still being optimized. Presumably the first detector station of the MVD will be located 5 - 10 cm downstream the target. It will use ultra thin and highly granular silicon pixel detectors while the STS relies on radiation hard, double sided strip detectors. It is still debated if some intermediate layers of very fast silicon pixel detectors might be beneficial for tracking.

CBM is designed as free running system using self-triggered detectors and high level event

*Speaker.

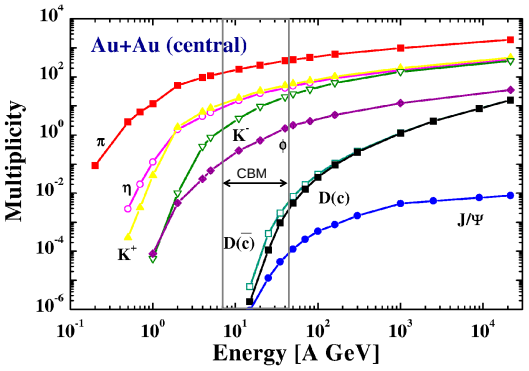

Figure 2:
The average number of mesons produced per central Au+Au collision (multiplicity) as a function of the incident beam energy. The calculation was performed with the HSD transport code. No in-medium mass modification was taken into account. As open charm (D) is produced close to the kinematic threshold in the SIS-300 energy range (10 - 40 AGeV), the production multiplicity is small and varies strongly as function of the beam energy. Figure from [4].

selection. The trigger concept for open charm measurements aims to pick up the zero suppressed data stream provided by the detectors and to reconstruct the event by performing tracking in the MVD and STS in real time. A scan for displaced decay vertexes is intended to allow for a selection of interesting events. The details of this tracking concept are still under debate. The task is complicated by the presence of displaced decay vertexes from the decays of strange particles.

2. Fundamental considerations on the requirements on the CBM-MVD

2.1 Beam time and collision rates

The requirements on the CBM-MVD are derived from two elementary needs, which are the production and the reconstruction of open charm. At SIS-300 energies, open charm production occurs close to the kinematic threshold. The multiplicities are therefore low and, due to a lack of experimental knowledge on the elementary cross sections, difficult to quantify from theoretical models. According to the predictions [4] shown in figure 2, we consider a production multiplicity of roughly $10^{-5} - 10^{-3}$ open charm particles of each species ($D^{\pm}$, D^0, Λ_C) per central Au+Au collision. Accounting for the branching ratio of the hadronic decay channels and assuming a reconstruction efficiency of few percent, one estimates that one may reconstruct roughly $10^{-8} - 10^{-6}$ open charm particles of each species per central collision. We aim to measure $\sim 10^{10}$ to 10^{12} central collisions to reconstruct roughly 10^4 open charm particles of each flavor per year.

It is planned that within one year, CBM will have $5 \cdot 10^6$ s (two months) beam on target. One requires therefore a minimum collision rate of $2 \cdot 10^3$ to $2 \cdot 10^5$ central collisions per second, which corresponds to $2 \cdot 10^4$ to $2 \cdot 10^6$ collisions integrated over all impact parameters. Using an 1% interaction target, this rate is in reach of the very high intensity values of the SIS-300 synchrotron. However, it introduces strong constraints on the time resolution and the radiation hardness of the detector system.

2.2 Radiation doses

In order to estimate the requirements on the radiation hardness of the MVD, the expected radiation doses for a vertex detector station located $z = 5$ cm and $z = 10$ cm downstream the target were simulated with GEANT-3[9] + GCALOR[10]. The results of this exploratory study were confirmed with a comparative study using FLUKA[11]. Both studies simulated radiation doses

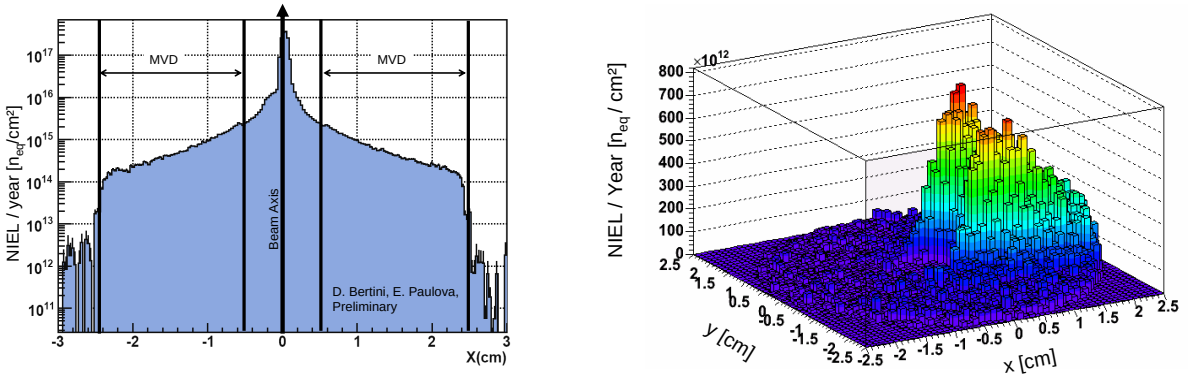

Figure 3:
Left: Radiation dose for a vertex detector station located 5 cm from the target. The beam axis and the region covered by the MVD station according to the CBM standard geometry is shown.
Right: The additional contribution caused by δ-electrons (see text).

obtained in 25 AGeV Au+Au collisions with random impact parameter, which were generated with UrQMD[12] . The non ionizing energy loss of the particles penetrating the detector stations were set according to the tables presented in [14]. The numbers were normalized assuming a beam intensity of 10^9 ions per second and a 1% target generating 10^7 collisions per second. The integrated yearly operation time of CBM was set to $5 \cdot 10^6$ s beam on target.

The preliminary results of the studies are shown in Figure 3 (left) for a detector station located at $z = 5$ cm. One observes that the radiation dose on the station is largest close to the beam axis. At the border of the beam hole of the detector station, it is up to $\sim 2 \cdot 10^{15}$ n_{eq}/cm^2 per year. Over the 2 cm covered by the station, the radiation dose drops by one order of magnitude.

We noticed that a sizable amount of δ-electrons are knocked out from our target by the primary beam. Despite a part of these electrons are deflected by the 1 Tm dipole field of the tracking magnet, they contribute substantially to the non-ionizing radiation. This contribution was simulated with GEANT-3 + GCALOR by shooting gold ions through the gold target of the experiment. The yield and spectrum of δ-electrons generated by this engine were checked against [15]. In the electron momentum region of interest between $p = 10$ MeV and $p = 100$ MeV, the simulation results were found to exceed the theoretical prediction by few 10%, what is neglected in the following. Again the damage factor of the electrons was set according to [14]. Despite their small damage factor in the energy region of interest ($0.05 - 0.09$ n_{eq}/cm^2), the electrons provide an additional radiation dose of up to $\sim 0.8 \cdot 10^{15}$ n_{eq}/cm^2 in the hottest areas of the detector. As illustrated in Figure 3 (right), the magnetic bending of the electron tracks distributes this radiation dose in a very asymmetrical way over the surface of the MVD station.

A station located at $z = 10$ cm would still receive a non-ionizing dose of $\sim 1 \cdot 10^{15}$ n_{eq}/cm^2 (plus $\sim 0.15 \cdot 10^{15}$ n_{eq}/cm^2 from δ-electrons).

The δ-electrons dominate by far the ionizing radiation dose in the vertex detector. Assuming that all charged particles penetrating the detector station are approximately minimum ionizing, the hottest region of a detector station located at $z = 5$ cm may accumulate ~ 340 Mrad per year. Additional magnetic deflection of δ electrons reduces this dose to ~ 80 Mrad for a station located at $z = 10$ cm.

2.3 Vertex resolution

Our main selection criterion for identifying open charm particles will be to separate their secondary decay vertex from the primary vertex. To do so, the vertex detector has to extrapolate the trajectories (i.e. of particle pairs) back to their intersection point, which is typically equal to the primary vertex. If both particles are decay products of an open charm particle, their intersection point is away from this primary vertex as the open charm particle traveled a certain distance before decaying.

In the previous section, we assumed a reconstruction efficiency of few percent for open charm mesons. Following this requirement, one can obtain a first impression about the necessary secondary vertex resolution of the detector. To do so we assume in a simplistic estimate, that CBM can trigger on central events. We consider for reasons of simplicity that the separation of the secondary vertex from the primary vertex should be the sole cut within the analysis. The indicated intersection points of particle pairs generated in the primary vertex should be distributed around this vertex according to a Gaussian distribution. Moreover, the velocity of the open charm particles should be equal to the center of mass velocity of the collision system. Be $z = 0$ cm the position of the target and thus of the primary vertex. According to the decay law, the distribution of the decay length of open charm is given with:

$$n_{\mathrm{s}}(z) = C_0 \cdot \exp\left(-\frac{z}{\beta\gamma \cdot c\tau}\right) \tag{2.1}$$

In this equation, which is illustrated in figure 4, z stands for the distance between the reconstructed secondary decay vertex of, for example, an D^0 and the primary vertex. C_0 is a normalization factor, which will cancel out in the following. The Lorentz boost of the center-of-mass for a beam energy of 25 AGeV is $\gamma = 3.8$, which allows us to set the velocity of the particles to $\beta \approx 1$ in the following.

In order to obtain a good reconstruction efficiency of 5%, we chose a parameter z_0 such that a fraction of 5% of all open charm particles are within the selection criteria $z > z_0$. This is fulfilled if:

$$F_{\mathrm{s}}(z_0) = \frac{A \cdot N_{\mathrm{S}}}{N_{\mathrm{All}}} = \frac{A \cdot \int_{z_0}^{\infty} n_{\mathrm{s}}(z)\, dz}{\int_{0}^{\infty} n_{\mathrm{s}}(z)\, dz} > 5\% \tag{2.2}$$

In the equation, N_{S} stands for the selected open charm particles, N_{All} stands for the total number of created open charm particles and $A \approx 0.35$ for the geometrical acceptance of CBM. The condition is fulfilled if:

$$z_0 \leq 2 \cdot \gamma \cdot c\tau \tag{2.3}$$

This result sets a first constraint on our cut.

In a next step we assume, that we want to reach a purity of the signal of $S/B = 1$. As explained above, $S = 10^4$ open charm particles have to be reconstructed and that therefore $B = 10^4$ background particles can be tolerated within the run. Assume that this run measured 10^{10} central Au+Au collisions with 25 AGeV. As each collision generates roughly 400 negatively charged and

500 positively charged particles, $2 \cdot 10^5$ combinations per collision are to be considered if two body decays are analyzed. The total background of a single run is therefore formed by $N_{\mathrm{BC}} = 2 \cdot 10^{15}$

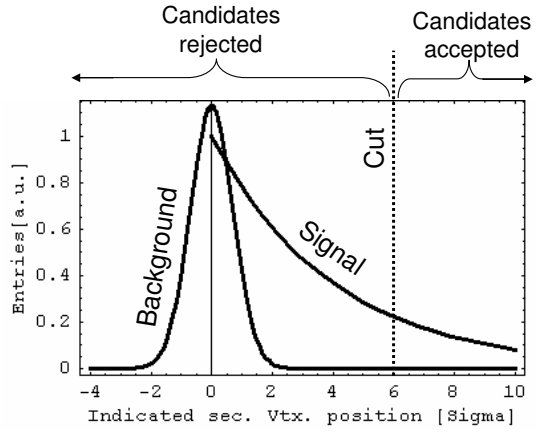

Figure 4:
Illustration of $n_{D^0}(z)$ (signal) and the corresponding background as a function of the reconstructed position of the displaced secondary vertex (z). This position is given in units of the secondary vertex resolution σ_{SvZ}. See text.

background candidates among which $N_{\mathrm{ABC}} = A \cdot N_{\mathrm{BC}} = 7 \cdot 10^{14}$ are geometrically accepted. The indicated origin of those pairs follows a Gaussian distribution with a width, which is equal to the secondary vertex resolution of the vertex detector σ_z. In order to reach a background of $B = 10^4$ only, the selection has to reduce it by a factor of $r \leq 7 \cdot 10^{-10}$. The relative number of entries above a certain cut z_0 in a Gaussian is given by:

$$r = \frac{1}{2} \cdot \left(1 - \mathrm{Erf}\left[\frac{z_0}{\sigma_z \cdot \sqrt{2}}\right]\right) \tag{2.4}$$

The condition $r \leq 7 \cdot 10^{-10}$ is fulfilled if:

$$z_0 \geq 6.1\ \sigma_z \tag{2.5}$$

Combining equation 2.5 and equation 2.3, one concludes that

$$\sigma_z = 0.3 \cdot \gamma \cdot c\tau \tag{2.6}$$

In order to reconstruct our most challenging observable, the Λ_C, reasonably well, we would need a secondary vertex resolution of:

$$\sigma_z = 0.3 \cdot \gamma \cdot c\tau(\Lambda_C) = 0.3 \cdot 3.8 \cdot 59.9\ \mu\mathrm{m} = 70\ \mu\mathrm{m}. \tag{2.7}$$

This value gives a first estimate for the requirements of CBM in terms of secondary vertex resolution.

It should be mentioned that the simplistic calculation shown here comes with several optimistic assumptions. In particular it neglects the presence of secondary decay vertexes originating from the decay of strange particles. Consequently, the detector performances suggested by the calculation are too optimist. Nevertheless, the approach provides a reasonable lower limit for the requirements of the detector system. Simulation results allowing for an estimate of the physics potential of the full detector system will be discussed in section 5.

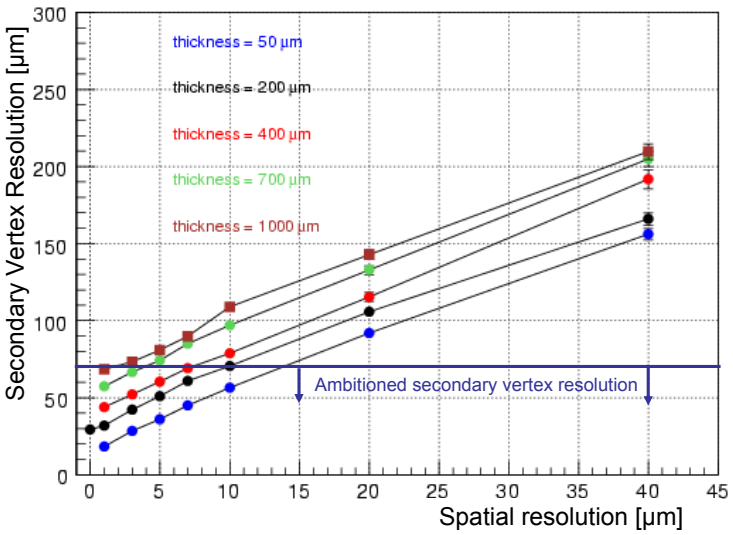

Figure 5:
The secondary vertex resolution of the CBM-MVD as function of the material budget (expressed in μm *silicon) and the spatial resolution of the detector. Note that* 1000 μm Si $\approx 1\%\ X_0$. *Only tracks with* $p > 1$ GeV/c *were accounted for.*

2.4 Spatial resolution and material budget

Systematic simulations and with CBMROOT [13] were performed in order to translate the requirements on the secondary vertex resolution into requirements of the detector. The secondary vertex resolution of the MVD was studied as function of the material budget and spatial resolution of the detector stations. Tracks having a momentum of $p \leq 1$ GeV/c were ignored as they are typically rejected within our data analysis for searching open charm signatures. The spacial resolution of the MVD stations was simulated with Gaussian smearing of the hit position. The results of the simulation for a first detector station located at $z = 5$ cm are shown in figure 5. One observes that the secondary vertex resolution of the MVD increases roughly linearly with the spatial resolution of the detector stations. A spatial resolution of $\sigma \lesssim 10$ μm (in both dimensions!) in combination with an ideally thin detector seems mandatory to fulfill the requirements of CBM. The hard maximum for the material budget would be $x \lesssim 1\%\ X_0$ for detectors with "ideal" spatial resolution. A realistic combination of both parameters would be a spatial resolution of $\sigma \approx 5$ μm and a material budget of of the detector stations of few $0.1\%\ X_0$ (corresponding to silicon with a few 100 μm thickness).

3. Technological constraints for the design of the MVD

3.1 Technological options

The requirements derived so far are listed in Table 1. They are valid for operating the Micro Vertex Detector at the CBM top luminosity, which is mandatory for open charm measurements closest to production threshold. Due to the higher production multiplicities, less stringent performances in terms of time resolution and radiation hardness are sufficient in order to do open charm physics at the higher beam energies of CBM. The table also provides information about the typical performances of established pixel detector systems like hybrid pixels and CCDs. Obviously, both detector concepts do not match the challenging requirements as the very radiation hard and fast hybrid pixel detectors do not reach the necessary spatial resolution and show a too large material

budget. The very light and granular CCDs miss the requirements in terms of radiation hardness by many orders of magnitude and would therefore fail within minutes due to radiation damage.

As the existing pixel detectors do not match the requirements of the CBM experiment, we searched for alternative technologies. The most promising candidates were found among the pixel detector systems being developed for the International Linear Collider (ILC), as this experiment has similar requirements in terms of granularity and material. Among the existing concepts, we identified DEPFETs [16] and CMOS Monolithic Active Pixel Sensors (MAPS)[18, 19, 20, 21] as most interesting options. We chose MAPS as non-exclusive guide line technology as their development had further progressed and as operating DEPFETs in our very inhomogeneous ionizing radiation fields appears challenging[1].

Comparing the performances of MAPS with the requirements of the CBM-MVD, one observes that the sensors cannot cannot match all requirements. However, they combine the strong points of CCD-detectors with a by three orders of magnitude higher radiation tolerance. MAPS were therefore considered to provide the best technological compromise available today. Therefore, we decided to work out, which part of the CBM physics program one might cover with this technology.

3.2 Features of Monolithic Active Pixel Sensors

CMOS Monolithic Active Pixel Sensors for charged particle tracking were initially developed for the vertex detector of the International Linear Collider by the IPHC Strasbourg. They were derived from sensors used for optical imaging. A single point resolution of $1-2$ μm and a detection efficiency close to 100% were routinely observed in beam tests at the CERN-SPS with various MAPS designs featuring up to 10^6 pixels on active areas as large as 4 cm^2.

Radiation hardness studies with different MAPS-prototypes [22, 23] showed that radiation significantly increases the leakage currents of the collection diodes of their pixels. A moderate cooling of the sensor allows keeping these leakage currents at a level where the corresponding shot

	Required$^{(1)}$	**Hybrid**	**CCD**	**MAPS**
Spat. resol. [μm]	$\lesssim 5$	~ 30 $^{(2)}$	~ 5 $^{(2)}$	$\lesssim 3$
Mat. budget [X_0]	few 0.1%	$\sim 2\%$ $^{(3)}$	$\sim 0.1\%$ $^{(4)}$	$\sim 0.05\%$ $^{(4)}$
Rad. hardn. [n_{eq}/cm^2]	few 10^{15}/year	$\sim 10^{15}$	$\sim 10^{10}$	$\gtrsim 10^{13}$
Time resolution	$\lesssim 100$ ns	25 ns	~ 50 μs $^{(5)}$	~ 20 μs

Table 1: Performances of different pixel detectors compared to the requirements for open charm meson reconstruction with full collision rate at CBM. The data on hybrid pixel detectors and CCDs was collected from [5],[6], [7] and [8].
Remarks: $^{(1)}$: For operating the MVD at the SIS-300 top luminosity. $^{(2)}$: Derived from the typical pixel pitch assuming digital readout. $^{(3)}$: ATLAS pixel module. $^{(4)}$: Sensor thickness. $^{(5)}$: Design goal for the International Linear Collider.

[1] DEPFET detectors demonstrated a competitive radiation tolerance against $\gtrsim 1$ Mrad [17]. However, operating the irradiated detector requires to adapt the gate voltage of the DEPFET in order to compensate its radiation induced threshold voltage shift. In vertex detectors with a collider geometry, one expects in first order a gradient in radiation doses in one dimension. This allows setting a common compensation voltage for all pixels of a line, which requires only moderately adapted steering chips. In contrast, the specific case of the CBM-MVD with its strong gradients in radiation doses in *both* chip dimensions might require to set a compensation voltage for each individual pixel. The latter would call for a steering logic of challenging complexity.

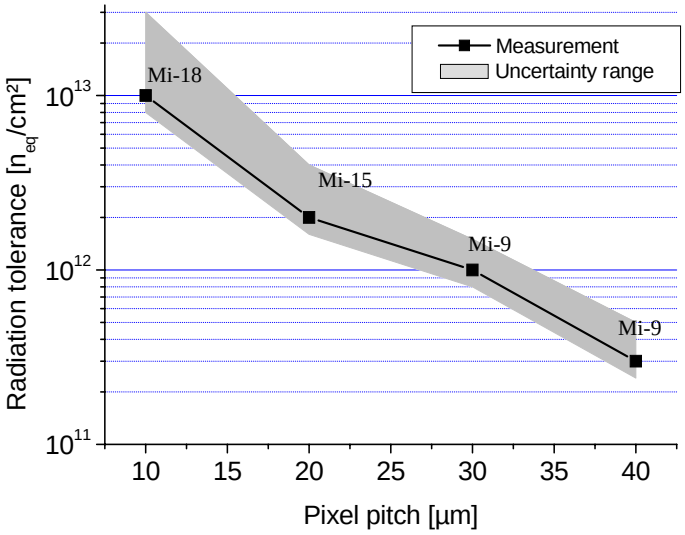

Figure 6: The measured tolerance of MAPS prototypes against non-ionizing radiation as function of the pixel pitch.

noise remains marginal. Rather a deterioration in the Charge Collection Efficiency (CCE), translating into a decrease of the S/N of the sensors, was identified as the key limitation for the radiation hardness of MAPS. A possible explanation is that an increased bulk damage in the epitaxial layer strongly reduces the lifetime of the diffusing charge carriers. It is considered that therefore the lifetime of the signal electrons in the sensor drops below the value required for collecting them by thermal diffusion. Shortening the diffusion paths by choosing a smaller pixel pitch alleviates this effect and allowed recently reaching a radiation tolerance against $\gtrsim 10^{13}$ n_{eq}/cm^2 [24].

Remarkably the correlation of the radiation tolerance of the sensors and the length of the diffusion paths turns into a correlation between this radiation tolerance and the pixel pitch of the sensors. This is illustrated in Figure 6 which shows the measured radiation hardness of MAPS-prototypes with different pixel pitch manufactured in the AMS 0.35 μm Opto process. An empirical fit of the measured data suggests that the radiation hardness of MAPS against non-ionizing radiation scales roughly according to:

$$T_{non-io} \approx 1.89 \times 10^{15}\ n_{eq}/cm^2 \cdot \left(\frac{P}{\mu m}\right)^{-2.27} \tag{3.1}$$

In this equation, T_{non-io} stands for the tolerance of the sensors against non-ionizing doses and P for the pixel pitch[2].

The radiation tolerance of MAPS against ionizing doses is currently given with 1 Mrad independently of the pixel pitch [26].

3.3 Sensor geometry and time resolution

MAPS are monolithic detectors which integrate the readout electronics and the sensor on the same, back thinned CMOS chip. Each pixel hosts a preamplifier located on top of the sensitive

[2]Note that the radiation hardness of MAPS depends on some parameters, which are specific to the CMOS process used for their production (namely the thickness of the epitaxial layer). Equation 3.1 does therefore not claim a general validity.

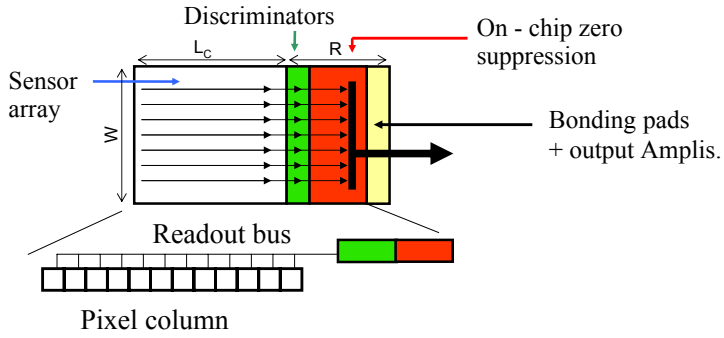

Figure 7: The concept of MAPS with massive column parallel readout. The signal of the pixels of each column is multiplexed on one readout bus and shipped towards a discriminator and data sparsification circuits located aside the pixel matrix. See text.

volume of the sensor, which is the epitaxial layer of the chip. A P-Well implantation hosting the transistors of the amplifier is used to isolate those transistors electrically from the sensitive layer. As any N-Well implantation other than one of the N-Well/p-epi collection diode would generate a parasitic charge collection, no PMOS transistors can be used in the sensitive surface. Because of this constraint, all logics requiring those transistors (for example discriminators) have to be placed at a separate surface outside the pixel matrix.

The readout of fast MAPS is therefore done in the massive column parallel way, which is illustrated in figure 7. The signal of the pixels of a column (or line) are multiplexed on one common readout bus and shipped to a discriminator being located aside the pixel matrix. The data of the discriminators is received by a digital data sparsification circuit which is to execute zero suppression. The compressed hit information is written out towards the DAQ of the experiment. The feasibility of this concept has meanwhile been demonstrated experimentally by building and testing the sensor matrix including the discriminators and, on a separated chip, the data sparsification circuits [27].

The concept of the chip readout introduces several constraints for the global design of the CBM-MVD. The most important one is a constraint in terms of time resolution and readout speed, which is caused by the limited bandwidth of the column readout bus. It is expected today, that this bus may allow for $f \approx 10^7$ readout processes per second[3]. The readout time t_{int} of a column with N_P pixels is therefore given with:

$$t_{int} = \frac{N_P}{f} \tag{3.2}$$

Equation 3.2 is of particular importance as it connects the time resolution of the pixel matrix with its geometrical surface. Knowing that each pixel has a pitch P, one can derive the maximum length L_C of the pixel matrix in one dimension. This is given with:

$$L_C = N_P \cdot P = t_{int} \cdot f \cdot P \tag{3.3}$$

The width W of a pixel matrix is constrained by the size of a reticle, which is between 20 and 30 mm depending on the CMOS process used for the production of the sensor.

The discriminators and data sparsification circuits are located aside the pixel matrix. The surface required for this logic in the direction of L_C is expected to be roughly $R = 1-3$mm. The readout electronics covers therefore a surface of $R \cdot W$. This surface is passive and needs to be covered by the pixel matrix of a second chip in order to reach a 100% fill factor in the MVD.

[3] A readout with $f = 6$ MHz is demonstrated with sensors manufactured in the AMS 0.35 μm Opto process.

Assuming that for reasons of material budget reduction, not more than two layers of silicon are acceptable, this pixel matrix must have the same surface than the surface covered by the readout electronics. From this constraint one derives the theoretical time resolution of MAPS, which is given with:

$$t_{int} = \frac{R}{P \cdot f} \tag{3.4}$$

Plausible values for the pixel pitch are between $P = 10$ μm and $P = 30$ μm. From this, one can derive the approximative time resolution of MAPS, which is given with $t_{int} \approx 10$ μs. As this time resolution is by up to a factor of 100 longer than the mean time between two collisions at the CBM maximum collision rate, one expects a pile-up of nuclear collisions in the MVD. Disentangling this pile-up is one of the major challenges for the tracking algorithms of CBM. It is considered to start the tracking at the most downstream STS detectors and to extrapolate identified tracks toward the MVD. Due to the very good granularity of MAPS, we suppose that a moderate pile-up of nuclear collisions will not translate into an excessive detector occupancy. However, track densities and the occupancy of the MVD is a crucial topic.

3.4 Track densities

In order to obtain a first estimate about the occupancy of the MVD, we performed simulations using CBMROOT framework and the GEANT-3+GCALOR engine. As already done for the radiation dose simulations, we accounted for two sources of particles, which are the the primary particles generated in the nuclear collisions and the δ-electrons, which are knocked out from the target by beam ions. The latter cannot be ignored as, unlike the faster hybrid pixel and strip detectors, MAPS pile up all δ-electrons produced between the nuclear collisions. Assuming a 1% interaction target, the particles of a primary collision are complemented by the δ-electrons produced by 100 heavy ions passing target. This makes those electrons a crucial contributor to the occupancy of the pixels.

We simulated the relevant track density under two assumptions. In the first simulation we assumed that the beam intensity is adapted in such a way to the ability of the detector, that the detector can distinguish the individual collisions. In this case, one will try to select central collisions and the occupancy of the detector is determined by the pileup of a central collision and the δ-electrons from 100 ions passing the target. In the second case, the detector will face higher beam intensities and therefore have to handle tracks originating from several nuclear collisions. As a selection of central collisions is not further feasible, this scenario is best described by merging δ-electrons with a central collision and further nuclear collisions with random impact parameter.

The preliminary simulation results for the track densities generated by central collisions are displayed in figure 8 (left). The figure shows the peak track density of MVD stations as function of the position of those stations. It should be mentioned that this track density shown is reached only at the small fraction of the detector, which is most intensely bombarded with δ-electrons. The results show that a station located at $z = 5$ cm will face track densities of up to 5 hits per mm^2 and collision already without pile-up. Knowing average number of firing pixels in a cluster of a MAPS detector is ~ 5 and assuming a small pixel pitch of $P = 10$ μm, this translates into an acceptable occupancy of $\sim 0.25\%$. A pile-up of 10 nuclear events, which corresponds to a beam intensity of $\sim 10^6$ collisions per second, would increase this occupancy to a considerably high value of $\sim 2.5\%$.

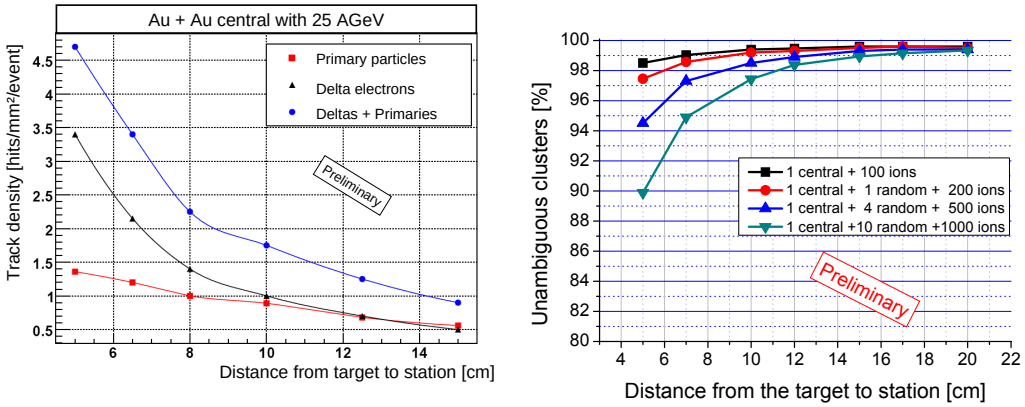

Figure 8:
Left: The peak occupancy of a MAPS based MVD as function of the position of this station for central collisions.As the final design of the MVD is not yet fixed, several potential positions for the detector stations were studied.
Right: Fraction of unambiguous clusters, which were well separated from clusters of neighboring tracks with respect to all clusters. The simulated events were composed by a pileup of a central collision, some collisions with random impact parameter and the delta electrons generated from 100 ions per collision. A pixel pitch of $P = 10$ μm was assumed.

Our worry concerning this occupancy is that reconstructed tracks might pick up a wrong hit of a merged cluster in the first detector station. Doing so might generate a slight modification of the track extrapolation, which turns into false indications of displaced decay vertexes. Given that CBM intends to trigger on those vertexes, already a modest amount of such cases might question the trigger concept.

The question whether the MVD shows a sufficient hit separation performance to exclude this scenario is being addressed with the newly developed MAPS digitizer. Among others, this digitizer simulates the charge sharing among the pixels of a cluster, a functionality which was calibrated with data collected from beam tests of MAPS with a 120 GeV/c pion beam at the CERN-SPS. Moreover, the the software package contains a low level cluster finding algorithm as it might be used in the future experiment. Both features allow a realistic simulation of the merging of clusters due to too high occupancies. First and preliminary results from an ongoing study suggest that hit merging is a crucial topic if the MVD operates with "big" pixels of 30 μm and a sizable pileup. However, as shown in figure 8 (right), a combination of a modest pile-up of below 10 events and the small pixels (10 μm) required for good radiation hardness reduces this effect substantially and more than 90% of all clusters well separated. Intense simulation work has been started in order to estimate the impact of the remaining, merged clusters on our tracking, the trigger concept and the signal reconstruction abilities of CBM.

3.5 Estimated power dissipation and the basic equation of MAPS

The power consumption of the MAPS pixels is strongly dominated by the one of the readout logic. This is as, except for the brief readout phase, the power consumption of a pixel is only $\lesssim$ 1pW while the end of column discriminators and data sparsification blocks have to operate continuously

to handle the incoming multiplexed data stream. For a first estimate of the power consumption of MAPS, one may thus state that the power dissipation of MAPS based detector scales with the number of columns required for using a unit of surface of the detector. To estimate this number, one has to know the surface of the individual column S_C, which is given with:

$$S_C = N_P \cdot P^2 \tag{3.5}$$

Here, N_P stands for the number of pixels in this column and P represents the pitch of those pixels, which are assumed as squared. We set $P_{col}(f)$ the power consumed by one end of column block and obtain a power density of a vertex detector surface:

$$\rho_{Power} = \frac{P_{col}(f)}{N_P \cdot P^2} \tag{3.6}$$

Note that equation 3.2 correlates N_P with the readout speed of the detector t_{int}. Merging both equations one obtains:

$$\rho_{Power} = \frac{P_{col}(f)}{t_{int} \cdot f \cdot P^2} \tag{3.7}$$

Introducing moreover the dependence of the radiation hardness from the pixel pitch (see equation 3.1) into this equation, one obtains:

$$\rho_{Power} = \frac{0.035}{\mathrm{m}^2} \cdot \frac{P_{col}(f)}{t_{int} \cdot f} \cdot \left(\frac{T_{non-io}}{\mathrm{n_{eq}/cm^2}} \right)^{0.88} \tag{3.8}$$

This equation links the most important parameter of the sensor technology, which is the radiation hardness, the integration time and the power consumption[4]. In case the pixel pitch is determined by the needs for good single point resolution σ, one can set (as suggested by the beam test results shown in [25])

$$\sigma = \frac{P}{5} \tag{3.9}$$

and one obtains:

$$\rho_{Power} = \frac{P_{col}(f)}{t_{int} \cdot f \cdot (5\sigma)^2} \tag{3.10}$$

The design of a MVD station has to provide the necessary cooling power to evacuate this heat load under vacuum conditions.

4. The design approach for the CBM-MVD

4.1 The design concept

In order to fulfill the requirements discussed in the previous section, the design of our detector ladders follows the concept shown in figure 9. This figure displays a ladder, which is formed by a mechanical support, silicon detectors and a heat sink, which is located outside the acceptance of the experiment. The mechanical support is composed from a sandwich of the ultra light Reticulated Vitreous Carbon (RVC) foam and the highly heat conductive Thermal Pyrolytic Graphite (TPG),

[4]Note that the restricted validity of equation 3.1 applies also to equation 3.8.

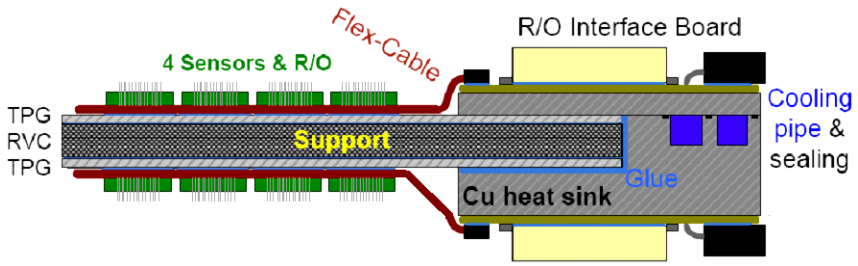

Figure 9: The conceptual design of a ladder of the CBM-MVD detector. The ladder is formed by a layer of RVC-carbon foam. Two layers of the highly heat conductive TPG transport the heat produced by the sensors toward a heat sink outside the detector acceptance. Flat band cables are used to bias the sensors and to transport the data to frontend boards located on top of the heat sinks.

which provides a very good heat conductivity of 1700 W/m/K at room temperature. While the RVC delivers the necessary mechanical stability, the TPG transports the heat produced by the sensors to the heat sink. The latter is cooled with conventional liquid cooling and, as it is located outside the detector acceptance, may contain a sizable amount of material.

The mechanical support hosts two layers of sensor chips. The sensors of each layer are arranged to overlap the passive surface of the sensors of the opposite layer, which allows to cover the planar surface of a MVD station with an (almost) 100% fillfactor. The biasing and the readout of the data produced by the sensors is done by by flat band cables located on top of the chips. The cables ship the data to some front end boards located on top of the heat sink. Those front end boards contain directly cooled low voltage regulators and a multiplexer logic. The latter is to concentrate the data on a minimum amount of optical or copper lines, which are passed through a vacuum window to the outside world.

4.2 Estimated material budget of the cooling support

The material budget of this detector ladder varies as function of the cooling power required as the cooling needs determine the necessary thickness of the TPG-layers. As starting point for the calculation of their thickness, we derive the temperature difference at a small element of the latter. The length of this volume along the latter is given with L_V. Its surface toward the neighboring element derived like $S_V = W \cdot \tau_V$ from the width W of the ladder and its thickness τ_V. We assume now, that this element is crossed by three different heat flows (see figure 10): P_1 is the heat injected

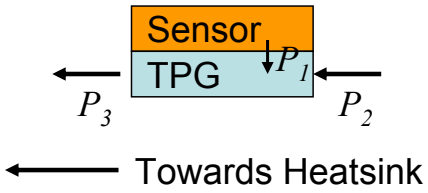

Figure 10: "Finite element" of the cooling support of the ladder. The heat streams used in the calculation are shown.

by the chips mounted on the volume element. P_2 is the heat flow, the element receives from its neighbors located upstream the latter. P_3 is the heat flow, the element sends to its neighbor directed toward the heat sink. For reasons of energy conservation, those heat flows fulfill the equation:

$$P_3 = P_1 + P_2 \tag{4.1}$$

A temperature gradient is required in order to drive the heat flow through our element. For very small volume elements in the middle of the ladder, it is justified to state that $P_2 \gg P_1$. For the calculation of the heat flow, we can therefore approximate that $P_3 \approx P_2$. The temperature difference ΔT_{V_i} on the volume number i is then derived according to the equation of heat conduction:

$$P_{3_i} = \frac{\lambda}{L_V} \cdot S_V \cdot \Delta T_{V_i} \tag{4.2}$$

$$\Rightarrow \Delta T_{V_i} = \frac{P_{3_i} \cdot L_V}{\lambda \cdot S_V} \tag{4.3}$$

In this equation, λ stands for the heat conductivity of the material.

In order to estimate the temperature drop on the full cooling support, one assumes that the volume element considered is the i^{th} element in a chain of equal volume elements. The element number zero is situated at the border of the latter, which is located opposite to the heat sink. As this element has no neighbors, $P_{2_0} = 0$. For the heat flow through the i^{th} element one derives then:

$$P_{3_i} = i \cdot P_1 \tag{4.4}$$

Knowing the heat density ρ_{Power} produced by the MAPS detectors (according to equation 3.7), one may derive P_1 from the dimension of the interface between the volume element of the sensor, which is given with $L_V \cdot W$:

$$P_1 = \rho_{Power} \cdot L_V \cdot W = \frac{P_{Block(f)} \cdot L_V \cdot W}{f \cdot t_{Int} \cdot P^2} \tag{4.5}$$

With this we conclude for P_{3_i}:

$$P_{3_i} = i \cdot \rho_{Power} \cdot L_V \cdot W \tag{4.6}$$

Combining this information with equation 4.3, one obtains:

$$\Delta T_{V_i} = i \cdot \frac{\rho_{Power} \cdot {L_V}^2 \cdot W}{\lambda \cdot S_V} \tag{4.7}$$

The temperature drop on the full ladder with a length of L is derived by summing up the temperature drops on the individual volume elements. This is done like

$$\Delta T = \sum_{i=0}^{L/L_V} \Delta T_{V_i} = \sum_{i=0}^{L/L_V} i \cdot \frac{\rho_{Power} \cdot {L_V}^2 \cdot W}{\lambda \cdot S_V} \tag{4.8}$$

Knowing that

$$\sum_{i=0}^{N} i \; = \frac{N(1+N)}{2} \approx \frac{N^2}{2} \tag{4.9}$$

one simplifies equation 4.8 to:

$$\Delta T = \frac{1}{2} \cdot \frac{\rho_{Power} \cdot L^2 \cdot W}{\lambda \cdot S_V} \tag{4.10}$$

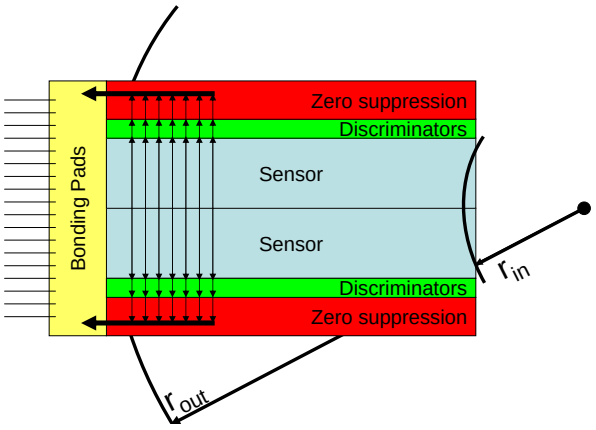

Figure 11: The sensor structure proposed for a use in the MVD. The surface of the station is covered by a large number of individually short readout columns. The bonding pads, and thus the cables, are located outside the detector acceptance.

As S_V was defined like $S_V = W \cdot \tau_V$, this translates into:

$$\Delta T = \frac{1}{2} \cdot \frac{\rho_{Power} \cdot L^2}{\lambda \cdot \tau_V} \tag{4.11}$$

$$\Rightarrow \tau_V = \frac{1}{2} \cdot \frac{\rho_{Power} \cdot L^2}{\lambda \cdot \Delta T} \tag{4.12}$$

Putting the energy density ρ_{Power} according to equation 3.8 and 3.10, one obtains:

$$\tau_V = \frac{0.018}{\mathrm{m}^2} \cdot \frac{L^2}{\lambda \cdot \Delta T} \cdot \frac{P_{col}(f)}{t_{int} \cdot f} \cdot \left(\frac{T_{non-io}}{\mathrm{n_{eq}/cm^2}} \right)^{0.88} \tag{4.13}$$

$$\Leftrightarrow \tau_V = \frac{1}{2} \cdot \frac{L^2}{\lambda \cdot \Delta T} \cdot \frac{P_{col}(f)}{t_{int} \cdot f \cdot (5\sigma)^2} \tag{4.14}$$

This equation defines the necessary thickness of the cooling layer as function of the detector requirements[5]. The radiation length of this layer can be derived knowing that TPG is a flavor of graphite.

For the calculation of the thickness of the cooling layer, we assume as a plausible scenario that the pixel detector will operate at a position of $z = 5$ cm ($\Rightarrow L = 2$ cm) with a pixel pitch of 10 μm and a time resolution of 20 μs. The power dissipation of an end of column block of a MAPS detector[6] is set to $P_{col} = 600$ mW. A temperature gradient of $\Delta T = 15$ K is accepted in order to drive this heat toward the heat sink. Using this input, we compute a $\tau_V = 250$ μm.

4.3 Material budget of a detector station

For the design of the crucial first detector station, one may profit from the small dimensions of this station. The acceptance of CBM requires the station at $z = 5$ cm to approximate a circle an outer radius of $r_{out} = 2.5$ cm and an inner hole[7] with a radius of $r_{in} = 0.5$ cm. The length of a detector ladder is therefore $L = 2$ cm and thus slightly below the typical size of a reticle used for designing

[5] Note that restrictions for the validity of equation 3.1 applies also to equation 4.13.

[6] Estimate for sensors manufactured in the AMS 0.35 μm Opto process. From [28].

[7] This inner hole is slightly enlarged with respect to the global inner acceptance angle of CBM in order to generate the necessary room for the beam and to reduce the radiation doses on the station.

Material	Functionality	X_0 [cm]	Thickness	x [%]
Silicon	Sensors	9.4	2×50 μm	0.11
TPG (Cooling)	Cooling	19.0	~ 250 μm	~ 0.13
RVC	Mech. support	723.7	3 mm	0.04
Glue	Integration	~ 35.0	4×30 μm	~ 0.04
Sum	Station	–	3.5 mm	~ 0.31

Table 2: Estimated material budget of a vertex detector station located at a position of $z = 5$ cm. The flat band cables used for readout do not contribute as they can be installed outside of the detector acceptance. Note that the radiation length of the glue and the thickness of the TPG depend on future technology choices.

a MAPS chip. This should allow to cover this station with sensors having the geometrical form shown in figure 11. This geometry combines the short columns required for a good time resolution with a width, which is sufficient for covering the surface of the MVD station. The bonding pads of the sensors (and the corresponding cables) are located outside the detector acceptance. The cables do therefore not contribute to the material budget of the system.

The remaining material budget is contributed by the 50 μm thick silicon of the sensors [29], the TPG of the cooling layers, four layers of glue and the RVC carbon foam used to stiffen the structure. An estimate of the corresponding material budget is shown in table 2, which suggests that a material budget of 0.3% X_0 is not out of scope for the crucial first station of the MVD.

5. The physics potential of the detector concept

5.1 Running scenario

Newly arising pixel detector technologies like SOI-detectors or pixel detectors based on 3D-VLSI have the potential to improve the limits of the pixel detector technology substantially within the next decade. However, experience shows that it needs a substantial amount of time to evolve a promising technology into a running detector. We suppose therefore that the promising next generation pixel sensors will become available only after the the start of CBM and foresee therefore two MVD generations.

The first MVD generation will rely on MAPS. Due to the existing experience with this technology, it will be available from the start of CBM. Given the limits of MAPS in terms of time resolution and radiation hardness, this detector will presumably not allow to cover the full physics program of CBM. However, it will open the door to the so far unknown world of open charm produced in p-p and A-A collisions at the SIS-300 top energies and thus allow for valuable physics programs. An upgraded MVD based on next generation sensors will presumably allow to complete the mission of CBM by measuring open charm also at lower beam energies.

We suppose that the first generation MVD will operate with a time resolution slightly slower than 10 μs in order to relax the requirements on cooling and material budget. A modest pile up of nuclear collisions should be tolerable and allows for a collision rate in the order of few 10^5 collisions per second. At this collision rate, the radiation tolerance of MAPS is sufficient for a reasonable operation time in the order of months. The option to produce MAPS in cheap industrial mass production will allow for a regular replacement of the small MVD stations, which further

increases the physics potential of the system. To limit the radiation damage in the detector, the MVD is removed whenever CBM operates on physics cases like di-muon spectroscopy, which do not need vertex information but require very high beam intensities.

The trigger system for open charm will rely on a real time tracking and on applying selection criteria on the impact parameter of individual tracks and on the secondary vertex on the fly. Higher level analysis may moreover use the hadron identification information from the time of flight system of CBM. The latter allows for a $\pm 2\sigma$ separation pions and kaons with a momentum of up to $p = 3.5$ GeV/c. Moreover, it may identify protons with good efficiency for $p \lesssim 6$ GeV/c[30], which covers most of the momentum range of interest.

5.2 Simulation of the physics performance

Various simulations were performed in order to estimate the physics performances of the MVD detector in the above discussed running scenario. The physic simulations typically relied on a open charm production with a thermal model and a generation of the underlying nuclear collisions with UrQMD. Event mixing of the nuclear collisions was required to reach the extremely high background statistics needed for testing the efficiency of our selection criteria.

The track finding and track fitting in the simulations was done using a cellular automaton track finder and a Kalmann filter. Both software packages, which are currently being optimized for multi-core processing architectures, are part of the CBMROOT simulation and analysis package. The main selection criteria applied were the impact parameter cut of the individual tracks and a cut on the secondary vertex position of the decay candidate. Moreover, we checked if the momentum vector of the reconstructed particle points to the primary vertex. Pile-up and δ-electrons were so far neglected as the software tools required for simulating both effects became available only recently. The results presented hold therefore under the assumption that an efficient track finding is possible despite the high detector occupancies.

The primary goal of our simulations is to optimize the design of our detector and to understand the consequences of different technology choices. The precise results of the simulations vary therefore depending on the precise assumptions made on the material budget and the lifetime of the MVD. A conservatively chosen example of a simulation result for the reaction $D^+ \rightarrow K^- + \pi^+ + \pi^+$ is shown in figure 12. This simulation assumes a relatively low[8] beam energy of 25 AGeV and a material budget of 0.3% X_0 for a station located at $z = 10$ cm, which combines a low production multiplicity for open charm with a modest secondary vertex resolution of $\sim 80\ \mu$m. Nevertheless, within the lifetime of an individual set of sensors, 5000 D^+ mesons are reconstructed with a $S/B = 0.4$. Those numbers are expected to increase by roughly one order of magnitude for SIS-300 top energies. Similar results were achieved for $D^0 \rightarrow K + \pi$ and for the four-body decay $D^0 \rightarrow K^- + \pi^+ + \pi^+ + \pi^-$. Despite its extremely small lifetime, the Λ_C baryon will presumably be visible at high beam energies. However, the number of reconstructed particles will remain modest and allow only for measurements particle yields. Nevertheless, the results seem sufficient to cover a substantial part of the physics program of CBM.

[8] In the sense of our running scenario.

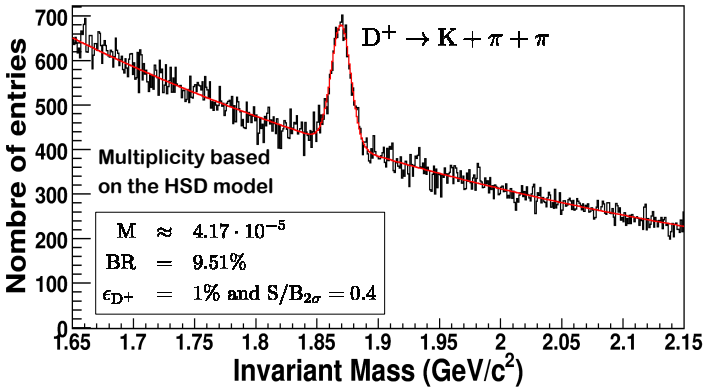

Figure 12: The peak of a reconstructed decay of $D^+ \to K^- + \pi^+ + \pi^+$ from a Au+Au collision at 25 AGeV. The amount of data shown corresponds to the lifetime of one set of MAPS sensors.

6. Summary and Conclusion

In this work, we introduced conceptual considerations for the micro vertex detector (MVD) of the Compressed Baryonic Matter Experiment (CBM). The CBM experiment is a fixed target experiment. The energy of its heavy ion beam of 8 - 45 AGeV is optimized to study the phase diagram of hadronic matter in the region of highest net baryon densities. The experiment aims to find for the expected first order phase transition of hadronic matter, signatures of chiral symmetry restoration and the critical endpoint of the phase diagram.

The aim of the MVD of CBM is to measure the production multiplicity and flow of open charm particles, which are so far unknown in this energy region. The particles will be reconstructed via their hadronic decay channels by identifying their secondary decay vertex. The latter sets unprecedented requirements on the performance of the detector. We motivated that an ideal MVD would have to provide a combination of very good spatial resolution (few μm), light material budget (few 0.1% X_0) and radiation hardness of (few $10^{15} \mathrm{n_{eq}/cm^2}$ + 340Mrad per year. A time resolution of $\lesssim 100$ ns is required to separate individual nuclear collisions at the CBM top collision rate of $\sim 10^7$ collisions/s.

The full set of requirements of the CBM experiment is not matched by any existing sensor technology. In order to approach them to the limits of nowadays technology, we chose the CMOS Monolithic Active Pixel sensors developed at IPHC Strasbourg as our non-exclusive guide line sensor technology. This was done as MAPS provide the necessary spatial resolution and light material budget together with an advanced radiation hardness of $\sim 10^{13} \mathrm{n_{eq}/cm^2}$. Concepts to reach a time resolution of $\sim 10\ \mu s$ were discussed.

Based on those numbers, we introduced a design concept for an MVD based on MAPS and discussed its features and limits. We showed simulation results which suggest, that the concept will allow for doing open charm physics at the CBM top energies with a reduced collision rate of few 10^5 collisions per second. This will be sufficient for for measuring the production multiplicity for the $\mathrm{D}^0, \mathrm{D}^{\pm}$-mesons and presumably for the Λ_C. Moreover, flow measurements might be possible for the open charm mesons. Those abilities make CBM an experiment with unique physics potential.

The CBM collaboration is observing closely the progress in the development of next generation pixel detectors based on novel technologies like the SOI-sensors or sensors relying on the

3D-VLSI integration. We envisage an upgrade of the MVD, once those promising sensors are available. The upgrade of this detector should expand its abilities sufficiently to complete the physics program of CBM also in the region of lower beam energies.

References

[1] FAIR Conceptional Design Report 2001, http://www.gsi.de/GSI-Future/cdr/

[2] http://www.gsi.de/fair/experiments/CBM/indedx_e.html

[3] V. Friese: "The CBM experiment at FAIR", PoS(CPOD07)056

[4] W.Cassing, E.L. Bratkovskaya, A. Sibirtsev: "Open charm production in relativistic nucleus-nucleus collisions", Nucl. Physics A 691 (2001) 753-778

[5] K. Arndt et al.: "Silicon sensors development for the CMS pixel system", NIM-A 511(2003) 106-111

[6] J. Grosse-Knetter on behalf of the ATLAS Pixel collaboration: "The ATLAS pixel detector", NIM-A 568 (2006) 252-257

[7] C.J.S. Damerell: "CCD-based vertex detectors", NIM-A 541(2005)178-188

[8] J. E. Brau: "Investigation of radiation damage effects in neutron irradiated CCD", NIM-A 541 (2005) 117-121

[9] R.Brun and F.Carminati:"GEANTŮDetector description and simulation tool", CERN Program Library Long Write-up W5013 (1993)

[10] C. Zeitnitz, T.A. Gabriel:"The GEANT-CALOR interface and benchmarc calculations of ZEUS test calorimeters" NIM-A 349(1994)106-111

[11] A. Fassò, et al., "FLUKA: a multi-particle transport code", CERN-2005-10, 2005, INFN/TC-05/11, SLAC-R-773.

[12] S. A. Bass et al.: "Microscopic Models for Ultrarelativistic Heavy Ion Collisions", Prog. Part. Nucl. Phys. 41 (1998) 225-370

[13] D. Bertini, M. Al-Turani, I. Koenig, F. Uhlig:"The FAIR simulation and analysis framework", J. Phys.: Conf. Ser. 119 Volume 119 (2008) 032011 (6pp)

[14] A. Vasilescu and G.Lindstroem, "Displacement damage in Silicon, online compilation." http://sesam.desy.de/members/gunnar/Si-dfuncs.html

[15] R.M. Barnett et al. :"Review of particle physics" PhysRev D V.54 Iss.1, pp. 1-708 (p.134)

[16] P.Fischer et al.:"Progress towards a large area thin DEPFET detector module", Nucl. Instr. Meth. A, **582**, 843 (2007)

[17] L. Andricek *et al.*: "The MOS-type DEPFET pixel sensor for the ILC environment", Nucl. Instr. Meth. A **565**,165 (2006).

[18] R. Turchetta, J. D. Berst, B. Casadei, G. Claus, C. Colledani, W. Dulinski, Y. Hu, D. Husson, J. P. Le Normand, J. L. Riester, G. Deptuch, U. Goerlach, S. Higueret and M. Winter:"A monolithic active pixel sensor for charged particle tracking and imaging using standard VLSI CMOS technology", NIM-A Volume 458, Issue 3, 11 February 2001, Pages 677-689

[19] G. Claus, C. Colledani, W. Dulinski, D. Husson, R. Turchetta, J. L. Riester, G. Deptuch, G. Orazi and M. Winter: "Particle tracking using CMOS monolithic active pixel sensor", NIM-A Volume 465, Issue 1, 1 June 2001, Pages 120-124

[20] Yu. Gornushkin *et al.*, "Test Results Of Monolithic Active Pixel Sensors For Charged Particle Tracking," Nucl. Instrum. Meth. A **478**, 311 (2002).

[21] G. Deptuch *et al.*, "Development of monolithic active pixel sensors for charged particle tracking," Nucl. Instrum. Meth. A **511**, 240 (2003).

[22] M. Deveaux, G. Claus, G. Deptuch, W. Dulinski, Yu. Gornushkin and M. Winter, "Neutron radiation hardness of monolithic active pixel sensors for charged particle tracking," Nucl. Instrum. Meth. A **512**, 71 (2003).

[23] M. Deveaux *et al.*, "Charge Collection Properties Of Monolithic Active Pixel Sensors (Maps) Irradiated With Non-Ionising Radiation," Nucl. Instrum. Meth. A **583**, 134 (2007).

[24] A. Besson *et al.*, "Achievements of CMOS Pixel Sensors for the CBM Micro-Vertex Detector", GSI Scientific Report 2007, Fair-Experiments-05, http://www.gsi.de/informationen/wti/library/scientificreport2007/

[25] Y.Degerli, A.Besson, G.Claus, M.Combet, A.Dorokhov, W.Dulinski, M.Goffe, A. Himmi, Y.Li, F. Orsini: "Development of binary readout CMOS monolithic sensors for MIP tracking" Nuclear Science Symposium Conference Record, 2007. NSS '07. IEEE, Volume: 2, On page(s): 1463-1470

[26] M.Deveaux: "Development of fast and radiation hard Monolithic Active Pixel Sensors (MAPS) optimized for open charm meson detection with the CBM - vertex detector", doctoral thesis, ULP Strasbourg - Goethe University Frankfurt (2008)

[27] M. Gelin et al.:"Intermediate Digital Chip Sensor for the EUDET-JRAI Beam Telescope", Proceedings of the IEEE-NSS, 2008

[28] C. Hu, IPHC, personal communication.

[29] M. Battaglia, D. Contarato, P. Giubilato, L. Greiner, L. Glesener, B. Hooberman: "A Study of Monolithic CMOS Pixel Sensors Back-thinning and their Application for a Pixel Beam Telescome", arXiv:physics/0611081 v1 8 Nov 2006, Submitted to Elsevier Science

[30] The CBM-collaboration: "Compressed Baryonic Matter Experiment - Technical Status Report", GSI (2005)